Perspective

Nanoparticle-Based Activatable MRI Probes for Disease Imaging and Monitoring

Yifan Fan, Limin Chen, Yuanxi Zheng, Ao Li, Hongyu Lin,* and Jinhao Gao*

Cite This: *Chem. Biomed. Imaging* 2023, 1, 192–204

Read Online

ACCESS | Metrics & More | Article Recommendations

ABSTRACT: Traditional diagnosis relies on identifying anatomical abnormality, which offers a stage for various anatomical imaging techniques, such as X-ray computed tomography (CT), ultrasonic imaging, and magnetic resonance imaging (MRI). The good capacity of providing anatomical details, especially for soft tissues, popularizes the clinical use of MRI. However, as the understanding of various diseases reaches the molecular level, it is gradually accepted that molecular anomaly often precedes anatomical abnormality. Therefore, molecular imaging, which is aimed at gathering various molecular information in organisms via imaging, starts to gain momentum. Unfortunately, traditional MRI is not capable of molecular imaging. As a result, there is an urgent demand for probes that enable MRI to "see" molecules. A promising design strategy for these probes is to elicit a signal change triggered by the presence of molecular targets, i.e. activation. Benefiting from the rapid development of nanotechnology, a number of nanoparticle-based activatable MRI probes have been developed for molecular imaging. This review summarizes recent advances of activatable MRI nanoprobes for imaging pathological characteristics of cancer, inflammation, and neurodegenerative diseases, with a focus on the design strategies and applications of these probes. In addition, the prospects and challenges of activatable MRI nanoprobes are also discussed.

KEYWORDS: *molecular imaging, MRI, activatable, nanoprobes, diagnosis*
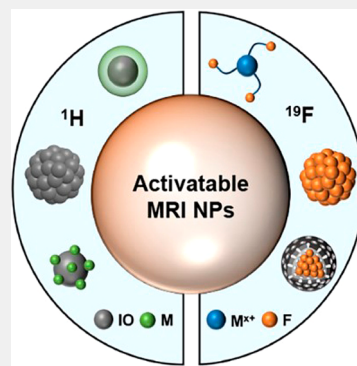
1. INTRODUCTION

Molecular imaging refers to visual detection of physiological and pathological processes at the cellular or molecular level to reveal the health status of tissues or organs through molecular information.[1,2] Since molecular changes often precede anatomical transition during disease progression, molecular imaging has attracted increasing attention as a more sensitive means than traditional anatomical imaging that has been widely used in the clinic, which stimulates the development of powerful imaging techniques, such as single photo emission computed tomography (SPECT)[3] and positron emission tomography (PET),[4] as well as the evolution of traditional imaging techniques, e.g., magnetic resonance imaging (MRI).[5]

MRI, which is a nonionizing imaging technique with high penetration, is one of the most powerful diagnostic tools for diseases.[6,7] Under an external magnetic field, ^{1}H MRI could present anatomical details and pathological information on organs and soft tissues with high resolution, because of the difference in water proton relaxation time in different tissues, which is now a pillar for medical imaging.[8,9] Contrast agents could further improve MRI sensitivity for subtle lesions by reducing the relaxation time of water protons for contrast enhancement. However, due to strong background signal interference, the capacity of ^{1}H MRI for imaging of some low concentration targets is limited. Meanwhile, ^{19}F MRI has been

gradually realized and accepted as a promising technique complementary to ^{1}H MRI due to [19]F's extremely low biological distribution (less than 10^{-6} M and only in bones and teeth), relatively high sensitivity (83% of ^{1}H), and a broad range of chemical shifts.[10,11] [19]F MRI is starting to gain momentum in some fields where ^{1}H MRI could not offer satisfactory results.

Over the past decades, various nanomaterials have been explored as MRI diagnostic tools because of their special structural and functional properties: (1) controllable size and morphology that allows tunable *in vivo* behaviors, such as extended blood circulation time and increased accumulation at certain sites and (2) surface functionalization that permits additional functionalities including enhanced biocompatibility and targeted delivery.[8,9,12] A number of nanomaterials with superior properties have been utilized as contrast agents (Gd, Mn, and Fe-based nanoprobes) for T_1 or T_2-weighted ^{1}H MRI, or ^{19}F probes (fluorocarbon, fluorinated ionic liquid, and
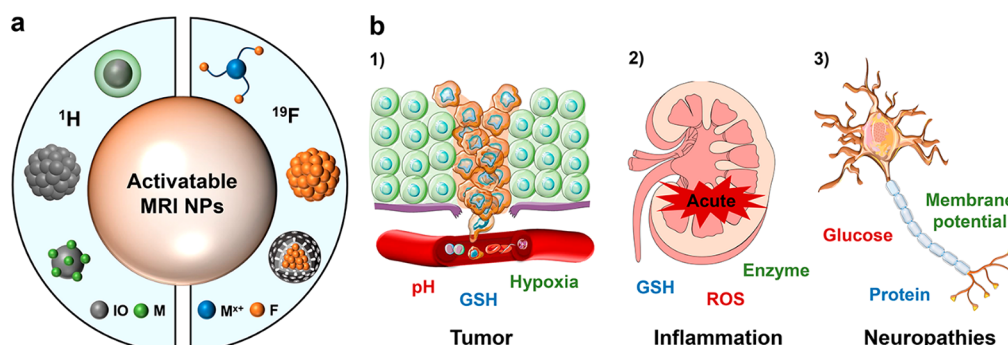
Figure 1. (a) A brief illustration of the major types of activatable ^1H and ^{19}F MRI nanoprobes for disease imaging and monitoring. IO: iron oxide; M: metal; M^{x+}: paramagnetic metal ions; and F: fluorine. (b) Three types of diseases discussed in this review. GSH: glutathione; ROS: reactive oxygen species.

inorganic fluoride-based ^{19}F nanoprobes) for "hot-spot" ^{19}F MRI with negligible background.[13−15] However, most of nanoprobes are designed based on an "always ON" pattern, which compromises their sensitivity due to increased background signals. A more effective design pattern is keeping probes "OFF" until they encounter certain stimuli. This design strategy, often referred as "activatable probes", minimizes potential background interference. Disease sites are often of distinct microenvironment characteristics that are different from normal tissues, which could be exploited as the triggers for probe activation. On the basis of this strategy, a series of biomolecule-activated MRI nanoprobes have been developed for visualizing various diseases. They remain "silent" before reaching the lesion sites. Once arriving at pathological microenvironments, these nanoprobes are activated by certain characteristic factors, which switches "ON" MRI signals. The contrast between lesion sites and normal tissues is therefore enhanced and allows real-time acquisition of molecular information for diagnosis and monitoring via MRI.[16−18]

In this review, we are committed to surveying the current research progress of activatable MRI nanoprobes, focusing on the nanoprobes for imaging tumor, inflammation, and neurodegenerative diseases (Figure 1). Their design strategies, working principles, and practical applications are all covered in detail. The discussion on their advantages and disadvantages are also included. Finally, the challenges and prospects of activatable MRI nanoprobes will also be briefly discussed.

2. IMAGING TUMOR BY ACTIVATABLE MRI NANOPROBES

Cancer is caused by anomaly in the cellular mechanisms that control cell growth and proliferation. At present, cancer remains one of the leading causes of death in the world. Solid tumors, the most common type of cancer, are abnormal tissues with complex biological microstructures, and special microenvironments, such as, hypoxia, acidosis, the up-regulation of glutathione (GSH) and hydrogen peroxide (H_2O_2) levels, etc.[12,19] Therefore, a series of stimuli-responsive MRI nanoprobes have been designed based on the characteristics of tumor microenvironment (TME) to provide more accurate biological information for tumors diagnosis.

2.1. Imaging Acidosis in Tumor

Compared with healthy tissues, TME hypoxia is caused by unlimited proliferation of tumor cells. Under hypoxic conditions, the upregulation in glycolysis and the down-regulation in oxidative phosphorylation lead to excessive lactic

acid, producing weakly acidic microenvironment surrounding most solid tumors, which is called the Warburg effect. The extracellular pH value of tumors is in the range of 6.0−7.0, while those of normal tissues and blood are maintained at around 7.4.[20,21] Consequently, the acidosis of TME is widely utilized to design pH-activatable MRI nanoprobes for tumor-specific imaging.

Several metal-based nanoparticles have been designed to construct pH-activated ^1H MRI nanoprobes, including Gd-based, Mn-based, and Fe-based pH-responsive MRI nanoprobes. Mn-based nanoparticles have attracted much scientific interest in the field of pH-responsive MRI nanoprobes due to that the responding product, Mn^{2+} with five unpaired 3d electrons, is known to be a relaxation-accelerating agent. For example, Song's group developed a pH-responsive nanoplatform (R-PtWMn) to store, deliver, and release Mn ions for MRI-guided ferroptosis therapy.[22] Under physiological conditions, few Mn ions were released from R-PtWMn, leading to low catalytic activity and weak MRI signals. After responding to acidosis, this nanoplatform caused significant signal changes for high-field T_1/T_2-weighted ^1H MRI, which enables the real-time visualization of Mn release and the monitoring of ferroptosis initiation. Recently, our group also developed a Mn-based activatable nanoprobe ($MnAsO_x@SiO_2$) for sensing pH (Figure 2a,b).[23] In this work, we chose water-insoluble manganese arsenite complexes as both a prodrug and a contrast agent. The complexes were encapsulated into hollow silica nanoparticles to form a pH-sensitive multifunctional drug delivery system. In acidic tumor microenvironments, manganese ions and arsenic trioxide were released, which dramatically increased T_1 signals, enabling real-time visualization and monitoring of arsenic trioxide release and delivery (Figure 2c−e). Besides, Ling and co-workers designed an MRI contrast agent highly selective to acidic tumor microenvironment for sensitive imaging of tumors (Figure 2f−h).[24] pH-sensitive nanoprobes (IONAs) were constructed by cross-linking iron oxide nanoparticles with hydrazone bonds. At neutral pH, IONAs are structurally robust, while in acidic TME, the hydrazone bonds were cleaved so that IONAs were quickly disassembled into small-sized iron oxide nanoparticles for contrast-enhanced T_1-weighted MRI (Figure 2i). These works have achieved encouraging results through ingenious structural design and effective probe construction to realize visual monitoring of tumors. However, as pH-sensitive ^1H MRI nanoprobes, the evaluation of biosafety from pH-induced leakage of metal ions is still a major concern despite the desirable results achieved *in vivo*. Besides, the lysosomal and
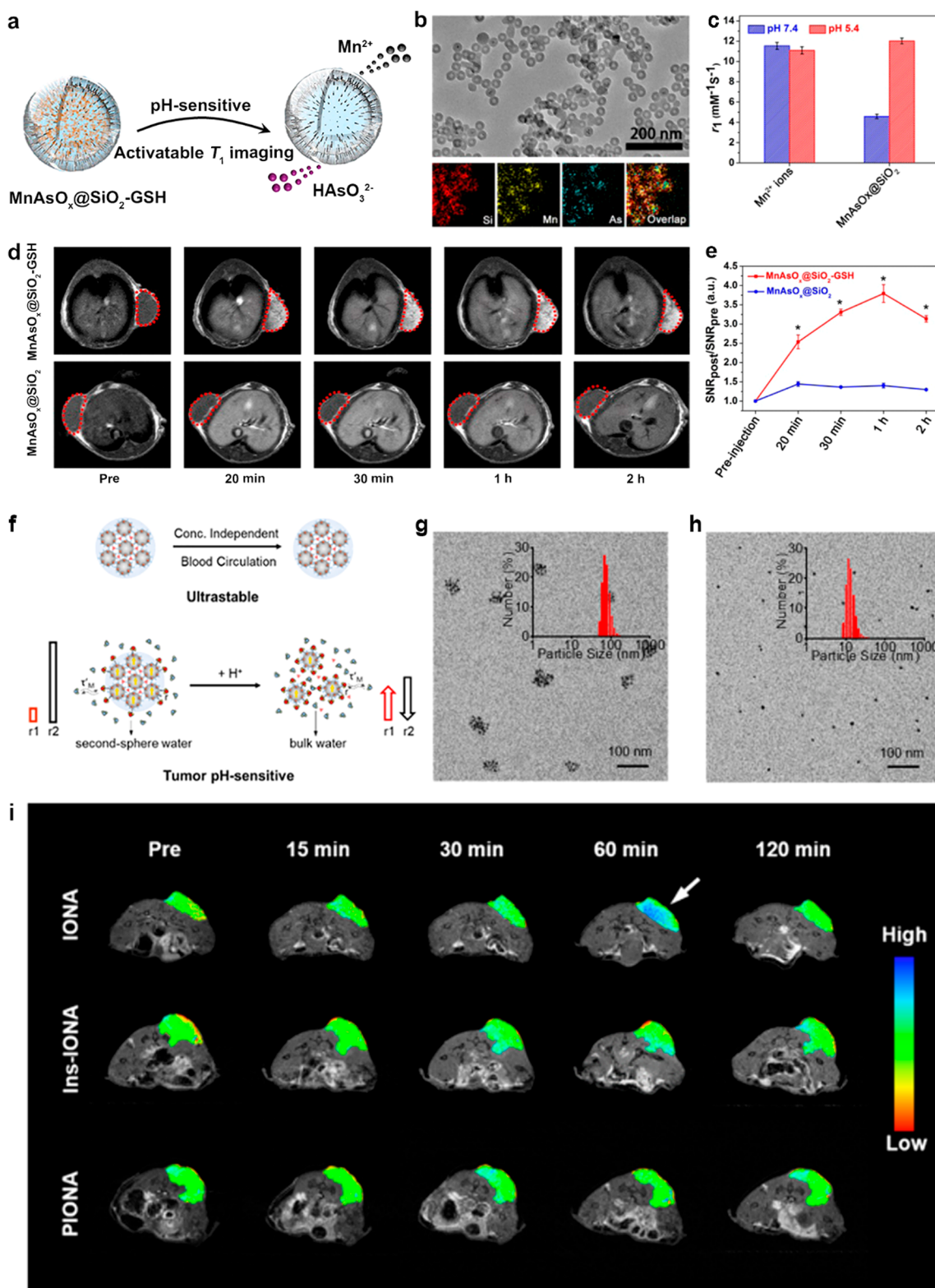
Figure 2. Imaging of tumor acidosis with activatable MRI probes. (a) Schematic illustration of the structure of $MnAsO_x@SiO_2$ and its pH-sensitive activation for T_1-weighted ^1H MRI. (b) Characterization of $MnAsO_x@SiO_2$ with TEM. (c) A comparison on the r_1's of Mn^{2+} and $MnAsO_x@SiO_2$ under different pH conditions. (d) T_1-weighted MR images of tumor-bearing mice at different time points after intravenous injection of $MnAsO_x@SiO_2$-GSH and MnAsOx@SiO_2. (e) Quantitative analysis on contrast enhancement corresponding to (e). Reprinted from ref 23. Copyright 2015 American Chemical Society. (f) Schematic illustration of pH-sensitive activation of iron oxide nanoparticle assemblies (IONAs) for MRI. TEM images of IONAs at pH 7.4 (g) and 5.5 (h) with size distribution analysis, respectively. (i) T_1-weighted MR images of tumor-bearing mice before and after intravenous injection of IONAs, Ins-IONAs, and PIONAs. Reprinted from ref 24. Copyright 2019 American Chemical Society.
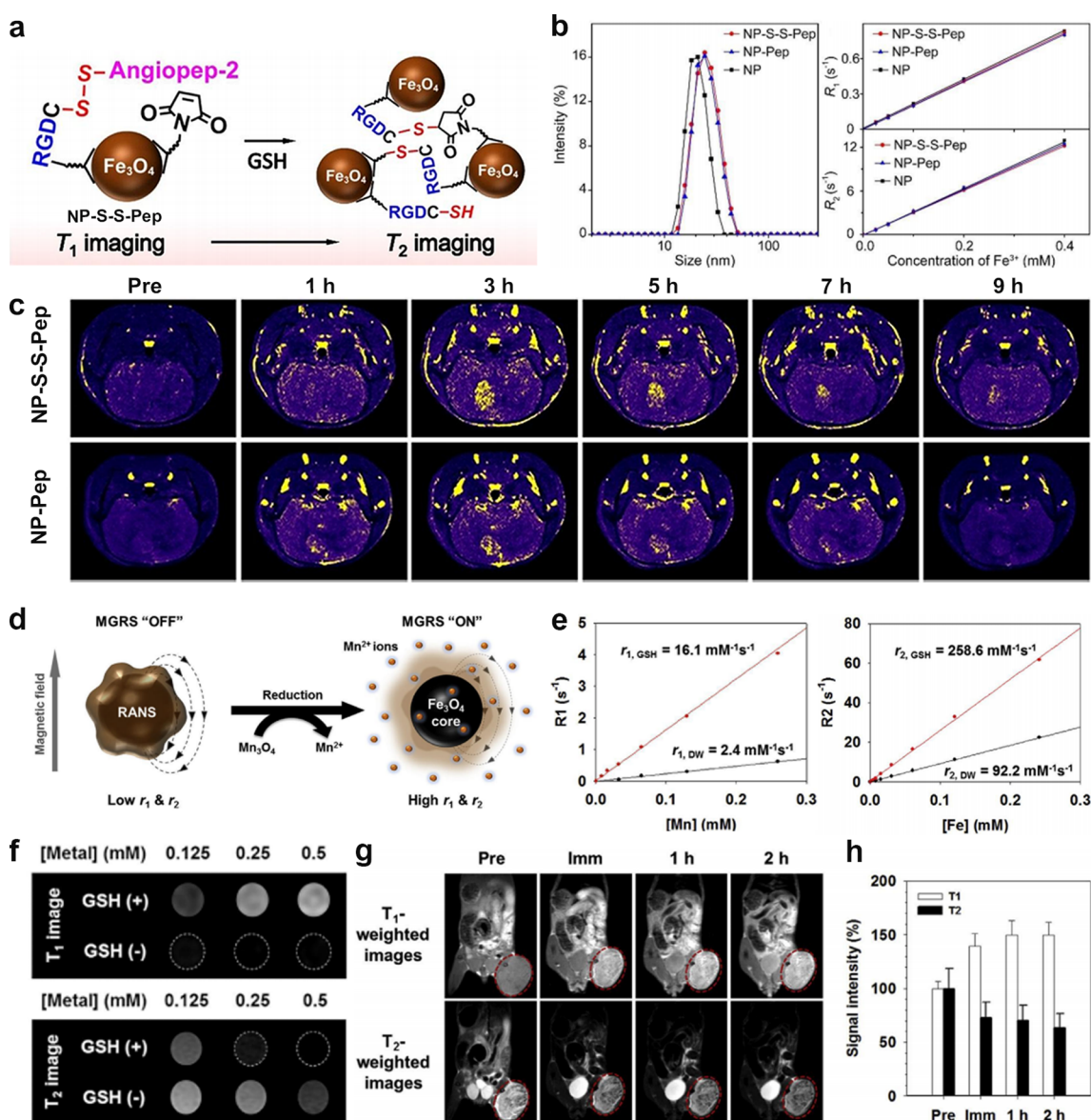
Figure 3. Imaging of GSH in tumor with activatable MRI probes. (a) Schematic illustration of GSH-induced agglomeration of responsive Fe_3O_4-based nanoprobes (NP-S-S-Pep). (b) Hydrodynamic size distribution and relaxation rate (R_1 and R_2) profiles of NP-S-S-Pep, NP-Pep, and NP, respectively. (c) T_1-weighted MR images of intracranial tumor-bearing nude mice before and after intravenous injection of NP-S-S-Pep and NP-Pep nanoprobes. Reprinted with permission from ref 27. Copyright 2021 Wiley. (d) Schematic illustration of redox-responsive activatable nanostarshells (RANS). (e) Relaxivity measurements of RANS. (f) T_1 and T_2-weighted MR images of RANS in the presence or absence of GSH. (g) T_1- and T_2-weighted MR images of MKN-45 tumor-bearing mice before and after intravenous injection of RANS. (h) Quantitative analysis corresponding to panel (g). Reprinted with permission from ref 28. Copyright 2016 Elsevier.

extracellular pHs are both within the acidic range in the tumor microenvironment, and whether pH-induced MRI signal changes are due to extracellular or lysosomal acidosis needs to be further investigated.

Meanwhile, a series of pH-activated ^{19}F MRI nanoprobes were also constructed by different groups. For example, Gao and co-workers reported pH-sensitive ^{19}F-MRI nanoprobes with tunable pH transitions to realize qualitative measurement of environmental pH values via ^{19}F-MRI.[25] Wang et al. designed pH-responsive ^{19}F MOFs by replacing the 2-methylimidazolate with 4-trifluoromethylimidazole. A significant enhancement in ^{19}F MRI signal intensities was observed when the pH was decreased from 7.4 to 5.5.[26] The pH-sensitive ^{19}F MRI nanoprobe has a promising potential as an alternative tool for ^1H MRI due to the absence of background

signal interference. However, the low fluoride content and long imaging time limit the sensitivity of ^{19}F nanoprobes. For the development of ^{19}F MRI nanoprobes, researchers should focus on optimizing the structure of the probes, optimizing the fluoride content, and increasing the field strength of the instrument to further expand the application scope of ^{19}F MRI.

2.2. Imaging of GSH Levels

Tumor cells could produce excess reducing substances during proliferative processes. As an important reducing agent, GSH could maintain the balance of intracellular redox reactions. Compared with normal tissues, the concentration of GSH in TME was up-regulated. Therefore, GSH-activated MRI nanoprobes have attracted wide attention for imaging tumor.
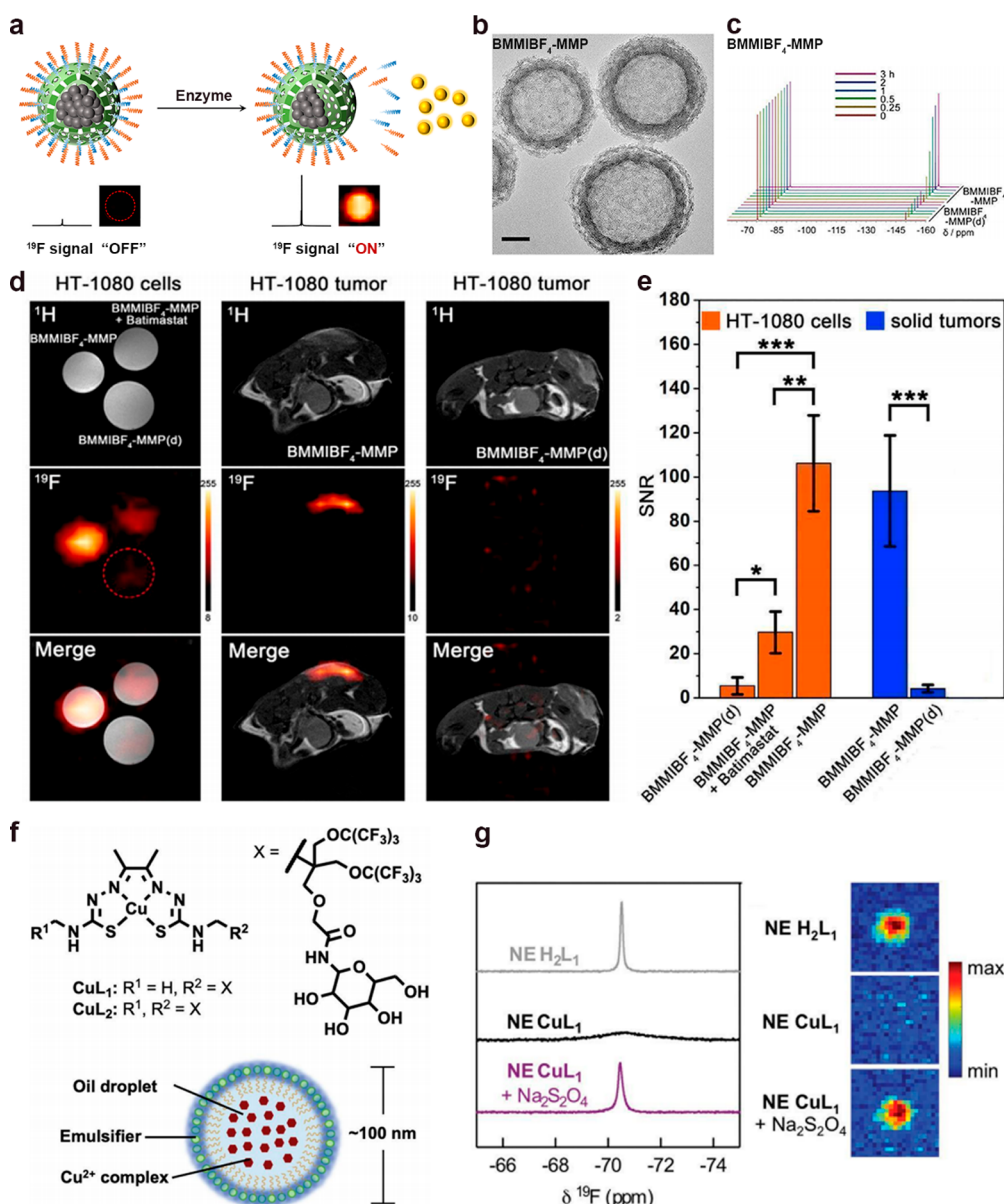
Figure 4. Imaging of enzyme overexpression and tumor hypoxia with activatable MRI probes. (a) Schematic illustration of fluorinated ionic liquid-based activatable ^{19}F MRI platform (FILAMP) for stimuli-responsive ^{19}F MRI. (b) TEM images of BMMIBF$_4$-MMP. (c) ^{19}F NMR analysis on the activation of BMMIBF$_4$-MMP in the presence of MMP-2. BMMIBF$_4$-MMP(d) containing a peptide that could not be cleaved by MMP-2 was used as a control. (d) Cellular and *in vivo* ^{19}F MRI with BMMIBF$_4$-MMP and BMMIBF$_4$-MMP(d). Batimastat was used as an inhibitor of MMP-2. (e) Quantitative analysis corresponding to (d). Reprinted with permission from ref 33. Copyright 2020 Elsevier. (f) Chemical structures of CuL$_1$ and CuL$_2$ and schematic illustration on the structure of CuL$_1$ or CuL$_2$-based nanoemulsions. (g) ^{19}F NMR and MRI analysis on the activation of NE CuL$_1$ in the presence of reductants. NE CuL$_1$ without reductants and NE H$_2$L$_1$ (pure ligands) were used as controls. Reprinted with permission from ref 34. Copyright 2020 Royal Society of Chemistry.

Nanoparticles consisting redox metal ions or disulfide bonds have been utilized to construct GSH-responsive ^1H MRI nanoprobes. Gao's group reported a GSH-responsive MRI nanoprobe (NP-S-S-Pep) to explore the correlations between the MR signals and GSH concentration in a mouse orthotopic brain tumor model, in which small Fe$_3$O$_4$ nanoparticles were linked with angiopep-2 peptides by disulfide bonds (Figure 3a−c).[27] After the disulfide bond was cleaved by GSH, the click reaction between a thiol group and maleimide residue could effectively induce the aggregation of Fe$_3$O$_4$ nanoparticles within TME. The concentration and heterogeneous distribution of GSH could be effectively assessed by T_1 and T_2-weighted MRI signals. Haam and co-workers reported a

rationally designed magnetic relaxation switch core−shell nanoprobe which consisted of a Fe$_3$O$_4$ core and a Mn$_3$O$_4$ shell for GSH activatable T_1/T_2-weighted ^1H MRI (Figure 3d).[28] In aqueous environment, the Mn$_3$O$_4$ shell acted as a protector to prevent Fe$_3$O$_4$ from interacting with water protons, and the Mn center was also hidden within the Mn$_3$O$_4$ structure, leading to quenched T_1 and T_2-weighted MRI signals. In TME, the Mn$_3$O$_4$ shell was reduced by abundant GSH. The resulting high-spin Mn^{2+} ions and exposed Fe$_3$O$_4$ cores could individually serve as MR contrast agents, leading to activated T_1 and T_2 signals (Figure 3e−h). GSH-regulated redox responsive nanoprobes based on disulfide bonds or redox metal ions provide a practical
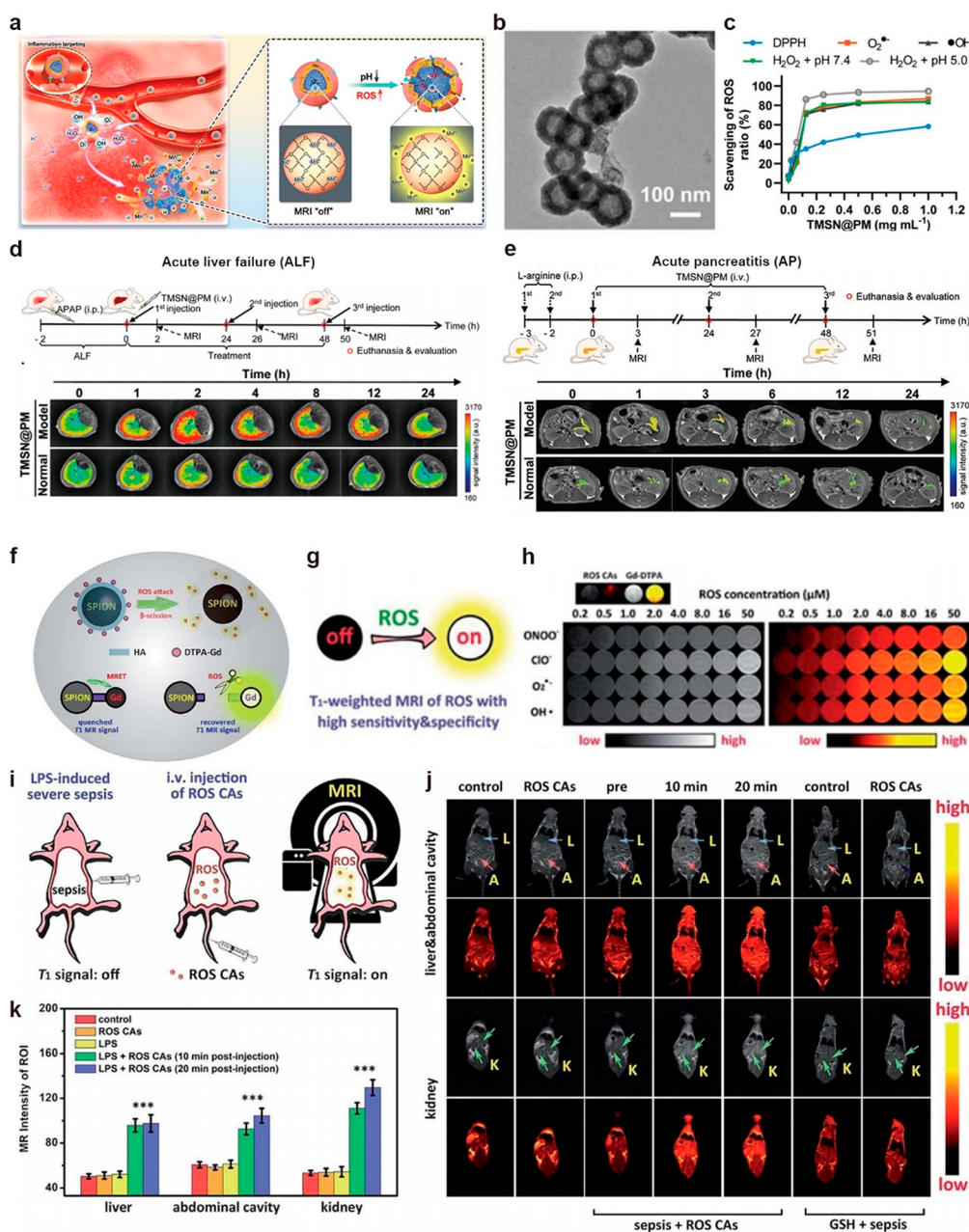
Figure 5. Imaging of ROS during inflammation with activatable MRI probes. (a) Schematic illustration of the mechanism of TMSN@PM for *in vivo* ^{1}H MRI-guided real-time monitoring of inflammatory diseases. (b) TEM images of TMSN@PM. (c) Scavenging efficacies of TMSN@PM toward DPPH, O_2^-, ·OH, and H_2O_2. In vivo monitoring of mice with established acute liver failure (ALF) (d) or acute pancreatitis (AP) (e) with TMSN@PM. Normal mice were used as controls. Reprinted with permission from ref 37. Copyright 2022 Wiley. (f) Schematic illustration of the detecting mechanism of ROS CAs. (g−h) T_1-weighted MR and corresponding pseudocolor images of ROS CAs solutions containing various ROS at indicated concentrations. (i) Schematic illustration of the establishment of a mouse model with severe sepsis by LPS and subsequent *in vivo* diagnosis of sepsis using ^{1}H MRI with ROS CAs. (j) *In vivo* T_1-weighted ^{1}H MR images of septic mice with indicated treatments. Normal mice were used as controls. (k) Quantitative analysis corresponding to panel (j). Reprinted with permission from ref 38. Copyright 2019 Royal Society of Chemistry.

means for *in vivo* imaging of GSH. The distribution of GSH in the tumor area can be assessed by analyzing the relationship between MR signal and GSH concentration, but it is challenging to accurately evaluate GSH concentration at the cellular level. At the same time, further evaluation is required for subsequent transformation and metabolic pathways of these nanoprobes after responding to GSH.

In the research of GSH-sensitive ^{19}F MRI nanoprobes, many works with clinical significance have been reported. In 2015, Kikuchi and co-workers developed a reduction-activated

perfluorocarbon nanoparticle (FLAME-SS-Gd^{3+}). The process of ^{19}F MRI signal from "OFF" to "ON" was achieved by controlling the distance of the Gd^{3+} complex and perfluorocarbons through redox reactions.[29] Besides, our group also developed a cascaded multiresponsive self-assembled nanoprobe by redox-triggered and near-infrared (NIR) irradiation-induced ^{19}F MR signal activation/amplification for sensing and imaging.[30] Due to the spin−spin relaxations and molecular mobility restriction, the ^{19}F NMR signal intensity of this probe was negligible. After the disulfides were cleaved by GSH, ^{19}F
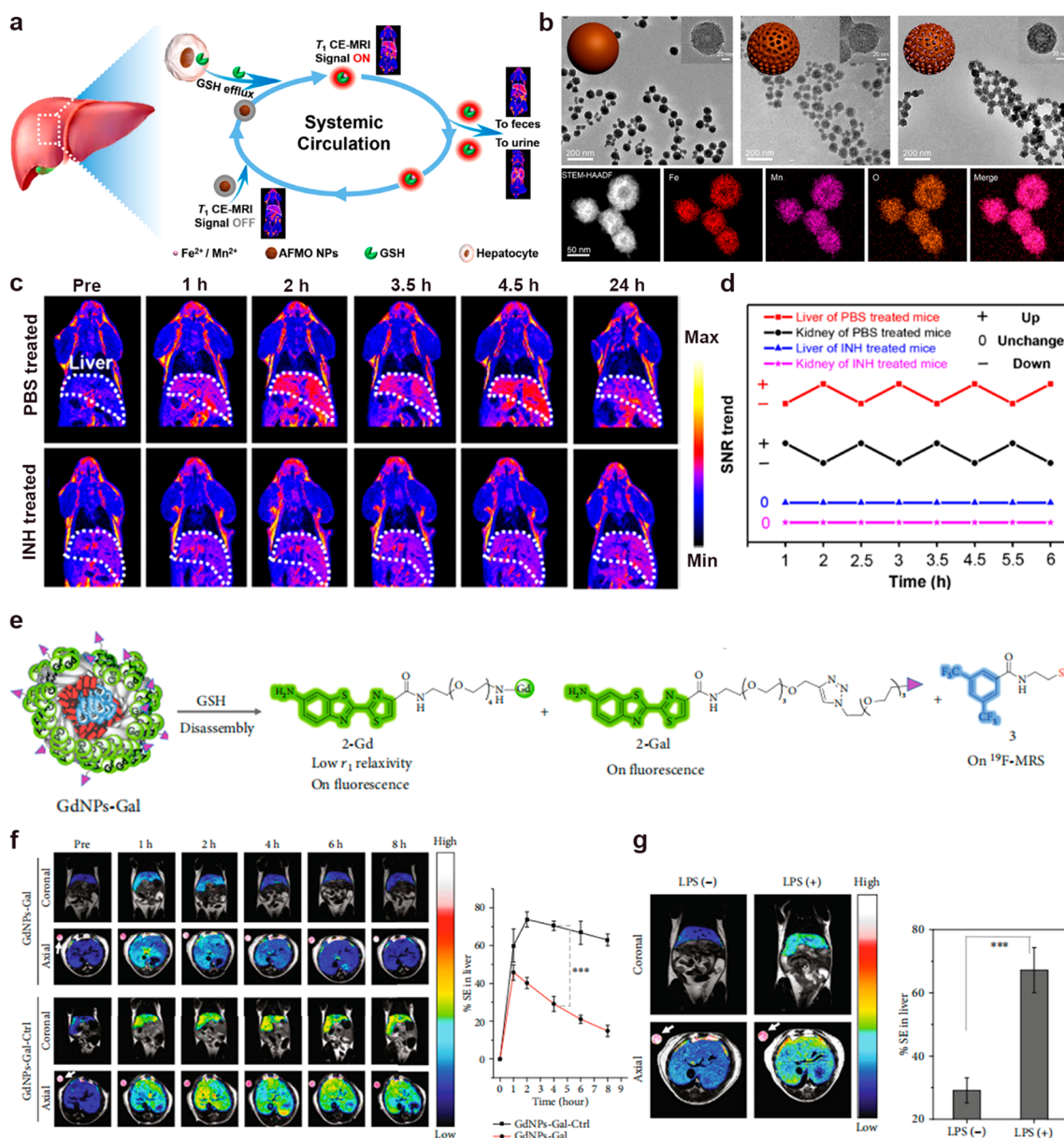
Figure 6. Imaging of GSH changes during inflammation with activatable MRI probes. (a) Schematic illustration of amorphous Fe_xMn_yO nanoparticles (AFMO NPs) for redox-activated contrast-enhanced T_1-weighted ^1H MRI. (b) TEM characterizations of AFMO NPs. (c) *In vivo* ^1H MRI of PSB-treated and INH-treated mice with AFMO NPs. INH treatment causes liver injury. (d) Trends of SNR changes in liver and kidney of the mice treated as indicated. Reprinted from ref 40. Copyright 2021 American Chemical Society. (e) Schematic illustration showing the mechanism of GSH-responsive GdNPs-Gal probes for in vivo imaging of liver inflammation. (f) T_1-weighted ^1H MRI of livers in healthy mice with GdNPs-Gal and GdNPs-Gal-Ctrl, the latter of which is a control probe that cannot respond to GSH and corresponding signal enhancement (SE) analysis. (g) T_1-weighted MR images and of livers in healthy mice (LPS (−)) or inflammatory mice (LPS (+)) and corresponding SE analysis. Reprinted with permission from ref 41. Copyright 2020 A Science Partner Journal.

signals were activated first by the weakening of intermolecular interactions and spin−spin relaxations. After laser irradiation, the signals were amplified by the further weakening of intermolecular interactions and spin−spin relaxations due to photothermal effects. Therefore, the ^{19}F signals were switched from "OFF" to "ON" by regulating the distance between the fluorine nuclei and the paramagnetic metal or among fluorine nuclei in the presence of GSH to achieve zero background imaging of the tumor. With the increasing fluoride concentration, these composite nanoprobes often exhibit considerable hydrophobicity, which significantly limits their further *in vivo* applications. Therefore, it is of great significance

to develop a hydrophilic and responsive ^{19}F nanoprobe with high fluoride content for potential clinical use.

2.3. Imaging of Other TME Characteristics

In addition to the acidic microenvironment and GSH overexpression, TME is often characterized by hypoxia, the up-regulation of ATP and H_2O_2 levels, and enzyme over-expression, etc. Song and co-workers developed ATP-mediated self-assembled Fe_3O_4 nanosystems (CACN) to monitor therapeutic processes.[31] Shi's group constructed a hyaluroni-dase-responsive MRI nanoprobe (TNS) with a distance-dominated property for specific tumor MRI.[32] Recently, our group reported a fluorinated ionic liquid-based activatable ^{19}F

MRI platform (FILAMP) for stimuli-responsive imaging (Figure 4a).[33] We encapsulated the fluorinated ionic liquid in hollow mesoporous silica spheres and then blocked the pores with MMP-responsive copolymers (Figure 4b,c). Because of the restriction of molecular mobility, the transverse relaxation of ^{19}F nuclei was considerably accelerated due to the strengthened homonuclear magnetic dipole−dipole interactions, resulting in negligible ^{19}F MRI signals. The ^{19}F MRI signals were enhanced when the polymeric shell was degraded by MMP which remarkably diminished homonuclear magnetic dipole−dipole interactions and slowed down the transverse relaxation. This result demonstrated the potential of FILAMP as a robust activatable ^{19}F probe for diagnosis and monitoring of biological and pathological processes (Figure 4d,e). Besides, Que et al. reported two highly fluorinated Cu-based imaging agents (CuL_1 and CuL_2) for detecting cellular hypoxia (Figure 4f,g).[34] The ^{19}F MR signals of both complexes were quenched due to paramagnetic Cu^{2+}, and the complexes displayed a large signal increase when the Cu^{2+} was reduced by hypoxia.

Due to the specificity of tumor tissues, TME-responsive nanoprobes have attracted wide attention in individualized tumor diagnosis. In spite of their good performance in tumor-specific imaging, significant progress still needs to be made to further improve their capacity to meet the demands of clinical translation. Combinational imaging of multiple TME characteristics might offer an interesting and promising direction for future development.

3. IMAGING OF INFLAMMATION PATHOLOGICAL CHANGES BY ACTIVATABLE MRI NANOPROBES

Inflammation is a basic immune process in which the body is stimulated by various injury factors (bacteria, viruses, injuries, etc.), leading to a defensive response.[35] Uncontrolled inflammatory reaction often causes a series of diseases. Inflammation microenvironments (IME) are mainly characterized by up-regulated ROS and pro-inflammatory cytokines and chemokines, overexpressed enzymes, and decreased reducing agents, etc. A series of biomolecule-responsive MRI nanoprobes have been developed for visualization of various factors in IME.

3.1. Imaging of Aberrant ROS in Inflammation

It has been revealed that inflammation responses are associated with aberrant ROS generation, including hypochlorite ions (ClO^-), hydroxyl radicals ($OH·$), superoxide anion radicals ($O_2·^-$), and peroxynitrite ($ONOO^-$).[36] Therefore, visualizing the distribution of ROS is a useful means for diagnosing inflammation and evaluating therapeutic outcomes, which could be achieved with ROS-responsive MRI nanoprobes.

Deng and co-workers designed a nanotheranostic agent (TMSN@PM) which composed with platelet membrane, tempol, manganese, and mesoporous silica nanoparticles for ROS-associated inflammation theranostics (Figure 5a,b).[37] In IME, TMSN@PM could scavenge the excess ROS to alleviate inflammation, leading to the gradual degradation of the nanoprobes to switch on T_1-weighted MRI signals by releasing Mn^{2+} ions. In addition, the relaxation changes are almost linearly correlated with the concentration of H_2O_2, which can reflect the degree of inflammation in real time (Figure 5c−e). Systemic ROS overproduction has been considered as an early characteristic of sepsis. Qu's group presented activatable nanoprobes (ROS CAs) composed of iron oxide cores (signal quencher), Gd−DTPA (signal enhancer), and hyaluronic acid
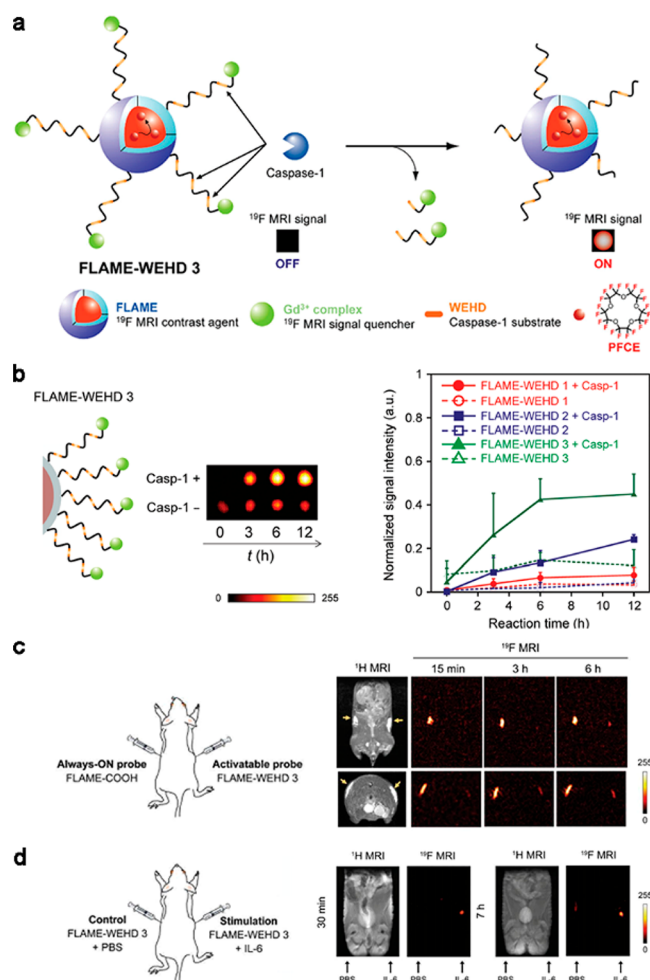

Figure 7. Imaging of enzymes during inflammation with activatable MRI probes. (a) Schematic illustration showing the mechanism of caspase-1-responsive ^{19}F MRI nanoprobes, FLAME-WEHD 3. (b) ^{19}F MRI of indicated phantoms and corresponding analysis on signal intensity. (c) ^{19}F MRI of a mouse treated with FLAME-COOH in the left flank and FLAME-WEHD 3 in the right flank. (d) ^{19}F MRI of a mouse treated with FLAME-WEHD 3 in the presence (in the right flank) or absence (in the left flank) of IL-6 stimulation. Reprinted with permission from ref 45. Copyright 2018 Royal Society of Chemistry.

(linker) for sepsis evaluation (Figure 5f).[38] In normal tissues, the T_1-weight MRI signals of Gd−DTPA were quenched by iron oxide. At sepsis sites, hyaluronic acid backbones were cleaved via b-scission reactions, and Gd−DTPA complexes were released from ROS CAs, leading to enhanced T_1-weight MRI signals. Thus, sepsis could be rapidly evaluated (Figure 5g−k).

Visual monitoring of ROS can effectively identify the location of inflammation and monitor the process of inflammation development. However, the complex design usually leads to the large individual variation of functional nanoparticles, which seriously affects the imaging reproducibility. Therefore, simple and effective nanoprobes are preferred. In addition, the biosafety of these probes should be further evaluated.

3.2. Monitoring of GSH Changes in Inflammation

In inflammation-related diseases, GSH is recognized as another important biomarker of liver inflammation, and several reports
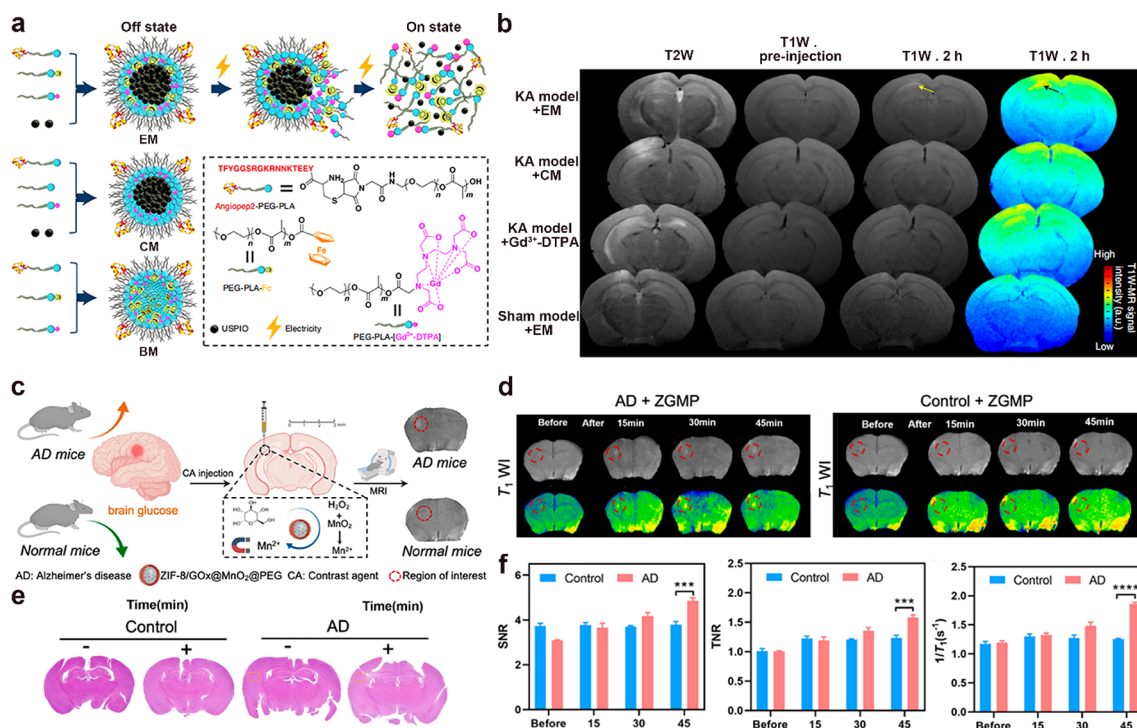
Figure 8. Imaging of neurodegenerative diseases with activatable MRI nanoprobes. (a) Schematic illustration showing the synthesis and sensing mechanism of an electrically responsive hybrid micelle (EM). CM: a control micelle (CM) without electrically responsive carboxyferrocene; BM: a blank micelle (BM) without the metallic cluster of ultrasmall superparamagnetic iron oxide (USPIO). (b) Coronal MR images of different models treated as indicated treatments. Reprinted with permission from ref 49. Copyright 2021 Springer Nature. (c) Schematic illustration of brain glucose-activated MRI contrast agents for early diagnosis of Alzheimer's Disease (AD). (d) T_1-weighted ^{1}H MR images and the corresponding pseudocolor images of AD and control mice treated as indicated. (e) H&E staining of AD and normal brains. (f) Comparison of SNR, TNR, and $1/T_1$ for the MRI results of normal mice and AD mice. Reprinted from ref 50. Copyright 2022 American Chemical Society.

have shown that the GSH level is significantly downregulated presumably because of the upregulation of ROS-production in inflammatory livers.[39] Noninvasive monitoring hepatic GSH levels is essential to early diagnosis and prognosis of acute hepatic injury. Our group developed an amorphous Fe_xMn_yO nanoparticles (AFMO-ZDS NPs) as redox-activated probes to visualize the dynamics of GSH-mediated biotransformation in liver with T_1-weighted MRI (Figure 6a,b).[40] In healthy liver tissues, T_1-weighted MR signals were significantly increased due to the degradation of AFMO-ZDS NPs, which released Mn^{2+} ions that were trapped by GSH to form metal-GSH chelates. In injured liver tissues, AFMO-ZDS NPs showed low T_1-weighted MR signals, which could be attributed to GSH depletion by excess ROS (Figure 6c,d). Therefore, the smart nanoprobes could also serve as a potent means for real-time assessment of liver function, which will substantially benefit early detection and accurate evaluation of liver injuries that are caused by diseases, drugs, toxins, or therapeutic agents under development. Besides, Ye's group reported a liver-targeted and GSH-responsive trimodal nanoprobe (GdNPs-Gal) for rapid evaluation of lipopolysaccharide-induced acute liver inflammation (Figure 6e).[41] In healthy hepatocytes, disulfide reduction and GdNPs-Gal disassembly were initiated by abundant endogenous GSH, leading to low ^{1}H MRI contrast but strong fluorescence and ^{19}F MRS signals. In hepatitis cells, downregulated GSH levels could slow the disulfide reduction and GdNPs-Gal disassembly, resulting in GdNPs-Gal with high r_1 relaxivity but quenched fluorescence and ^{19}F MRS signals, which generates high MR contrast, enabling noninvasive

visualization of LPS-induced liver inflammation via high-resolution MRI (Figure 6f,g).

Liver diseases caused by hepatitis are a serious threat to people's health. Acute hepatitis can lead to liver dysfunction and even death, so accurate diagnosis by molecular information is helpful for early diagnosis and prognosis. The GSH level in the liver can be assessed by MRI signal changes, allowing visual diagnosis of inflammation progression by these stimulus-responsive nanoprobes. Unfortunately, most of these nanoprobes contain Gd-based and Mn-based contrast agents which could cause significant toxic side effects due to the leakage of metal ions. Therefore, it is important to design safer and more sensitive GSH-responsive nanoprobes for accurate diagnosis by evaluating GSH levels.

3.3. Enzyme Biomarkers in Inflammation

Other than ROS and GSH, enzyme overexpression is also a major feature of IME. Common overexpressed enzymes includes aspartate aminotransferase (AST),[42] myeloperoxidase (MPO),[43] and cysteine proteases (e.g., caspase-1),[44] etc. Kikuchi and co-workers designed activatable ^{19}F MRI nanoprobes (FLAME-WEHD 3) for sensing caspase-1 activity.[45] In this sensor, Gd^{3+} complexes and caspase-1 substrate peptides (WEHD) were conjugated to the surface of fluorinated ionic liquid-based activatable ^{19}F MRI platform (FLAME), which composed of perfluoro-crown-5 ether (PFCE) core and a robust silica shell (Figure 7a). The ^{19}F MRI signals of PFCE were quenched because the T_2 was significantly shortened by the PRE effect of the Gd^{3+} complexes. When the peptides were cleaved by caspase-1, the ^{19}F MRI signals were activated due to

the release of Gd^{3+} complexes from the surface of FLAME (Figure 7b−d).

It is worth mentioning that this is the first ^{19}F MRI nanoprobe for detecting caspase-1 activity. However, the caspase-1-responsive ^{19}F nanoprobes did not show good imaging performance *in vivo* due to the influence of the enzyme concentration and biocompatibility. Based on the overexpression of enzymes in IME, peptide-assembled nanoprobes with higher biosafety and response specificity for visualizing the inflammatory process may be an interesting and promising strategy.

4. TRACKING NEURODEGENERATIVE DISEASE BY ACTIVATABLE MRI NANOPROBES

Neurodegenerative diseases (ND) is a type of illness caused by neural dysfunction, such as Alzheimer's disease (AD), Parkinson's disease (PD), and epilepsy, which seriously affect the health of the elderly. In accordance with the statistics of 2018, the prevalence of AD and PD are 3.20% and 1.06% for those who are over 60 years old in China, respectively.[46] In addition, the neurodegenerative microenvironment (NME) are characterized by neuroinflammation, metal ions disequilibrium, ROS, and protein accumulation, etc.[17] Due to low utilization and poor targeting, traditional drugs often fail to provide accurate diagnosis and effective treatment for ND. Therefore, a series of nanoprobes have been developed to penetrate the blood-brain barrier (BBB) and achieve diagnostic purposes. Among them, stimuli-responsive nanoprobes are considered as a promising means to achieve successful diagnosis through sensitive transitions triggered by NME characteristics.[47,48]

Epilepsy refers to a type of brain disorder characterized by abnormally excessive neuronal electrical activity. The abnormal membrane potential in the brain can also be utilized to diagnose and visualize the epileptogenic zone by MRI.[49] Li and colleagues developed a distance-dependent electro-responsive MRI nanoprobe, which consists of a paramagnetic polymer coating (signal enhancer) encapsulating ultrasmall superparamagnetic iron oxide (USPIO, signal quencher) for the facile MRI of epileptic foci in a kainic acid-induced epileptic mice model (Figure 8a).[49] The T_1-weighted MR signals of the nanoprobes were quenched in normal brain tissues due to the magnetic moment of USPIO which counteract the contrast enhancement effect of Gd^{3+}-DTPA. The excessive neuronal discharge triggered the breakdown of the nanoprobes, resulting in that Gd^{3+}-DTPA was drawn away from the quencher, which restored the T_1-weighted MR signals (Figure 8b). The distance-dependent electro-responsive MRI nanoprobes may increase the probability of detecting seizure foci in patients and provide more insights for brain diseases associated with epilepsy.

AD is one of the most common neurodegenerative diseases characterized by neuronal loss, which causes memory deterioration and dementia. Recent studies suggest brain glucose is an important biomarker of AD, which could be utilized for early AD diagnosis. Zhao's group developed a glucose activatable MRI nanoprobe (ZGMP) for the facile MRI of AD (Figure 8c).[50] The glucose-responsive nanoprobes consisted of ZIF-8, glucose oxidase, MnO_2 nanosheet, and PEG. In the model of AD, glucose could be recognized by glucose oxidase and generate H_2O_2. H_2O_2 reduced MnO_2 to Mn^{2+}, which shortened the relaxation time of surrounding water protons and resulted in enhanced MRI signals (Figure 8d−f). This smart nanoprobe allows for accurate diagnosis of

AD. However, the stability of ZIF, and the encapsulation efficiency of glucose oxidase still have room for improvement.

MRI is a powerful noninvasive method for the diagnosis of neurodegenerative diseases due to its high penetration and excellent resolution. Activatable MRI nanoprobes for imaging ND must meet more stringent requirements, including high imaging performance, low toxicity, BBB crossing, and favorable targeting ability. Currently, these types of nanoprobes are still facing a long road before clinical use.

5. SUMMARY AND OUTLOOK

MRI is undergoing a fast development from nonspecific physical imaging to specific biomolecular imaging. With the

Table 1. Representative Smart Nanosystems for ^1H/^{19}F MRI of Different Diseases[a]

disease type	responsive mode	nanosystems	imaging mode	ref
tumor	pH	PtWMn NPs	^1H MRI	22
		$MnAsO_x@SiO_2$		23
		Fe_3O_4 NPs		24
		^{19}F copolymers	^{19}F MRI	25
		^{19}F ZIF-PEG NPs		26
	GSH	Fe_3O_4-S-S-peptides	^1H MRI	27
		$Fe_3O_4@Mn_3O_4$		28
		FLAME	^{19}F MRI	29
		^{19}F self-assembly NPs		30
	ATP	Fe_3O_4 NPs	^1H MRI	31
	enzyme	$Fe_3O_4@Gd$	^1H MRI	32
		ionic liquid@SiO_2	^{19}F MRI	33
	hypoxia	nanoemulsions	^{19}F MRI	34
inflammation	ROS	$Mn-SiO_2@PM$	^1H MRI	37
		$Fe_3O_4@Gd-DTPA$		38
	GSH	Fe_xMn_yO NPs	^1H MRI	40
		Gd-based NPs		41
	enzyme	FLAME	^{19}F MRI	45
neurodegenerative disease	potential	Fe_3O_4 NPs	^1H MRI	49
	glucose	ZIF	^1H MRI	50

[a]Abbreviations: NPs, nanoparticles; PFOB, perfluorooctyl bromide; FLAME, fluorine-accumulated silica nanoparticle for MRI contrast enhancement; PM, platelet membrane; and ZIF, zeolite imidazolate framework.

rapid development of nanotechnology, MRI nanoprobes have made great progress in the past decades. A series of biomolecule-activated MRI nanoprobes have been constructed for imaging various diseased tissues, which provides more accurate and comprehensive information for disease research and diagnosis, representing a promising direction for the further development of MRI probes. In this review, we discussed the research situation of activatable MRI nanoprobes for tumor, inflammation, and neurodegenerative diseases, respectively, focusing on the strategies for their design. The composition and activation factors of each nanoprobe and the types of diseases are summarized in Table 1. The successful applications of these preclinical MRI nanoprobes demonstrate that the significant benefits of collecting both anatomical details and molecular information simultaneously will revolu-

tionize the current diagnostic paradigm which often gathers them separately. However, there are still several grand challenges that need to be solved for accelerating their clinical translation. The sensitivity of activatable ^{1}H MRI is significantly compromised by the high ^{1}H signal background in living organism while the sensitivity of activatable ^{19}F MRI only allows it for detecting biomolecules at millimolar or submillimolar levels. Besides, the scope of activatable MRI only covers a few types of disease, which needs to be substantially extended to meet the demand of the era of molecular imaging. Furthermore, more comprehensive safety assessment of these nanoprobes needs to be carried out to facilitate their preclinical studies and even clinical trials, including but not limited to their biodistribution, biocompatibility, biodegradability, pharmacokinetics, etc. Fortunately, some potential solutions have been proposed to address these problems, such as improving the magnetic field strength and developing high-efficient pulse sequences. It is noteworthy that some promising design strategies are on the horizon. For example, amplification, a common strategy that has been used in many probes for other analytical techniques, is rarely implemented for activatable MRI nanoprobes, which could be a game changer for the sensitivity problem. Collectively, these exciting advances and promising directions for further development clearly demonstrate that responsive MRI nanoprobes are looking at a prosperous future for accurate disease diagnosis in the future.

■ AUTHOR INFORMATION

Corresponding Authors

Hongyu Lin − *The MOE Laboratory of Spectrochemical Analysis & Instrumentation, Fujian Provincial Key Laboratory of Chemical Biology, and Department of Chemical Biology, College of Chemistry and Chemical Engineering, Xiamen University, Xiamen 361005, China;* ● orcid.org/0000-0002-5675-8537; Email: hylin007@ xmu.edu.cn

Jinhao Gao − *The MOE Laboratory of Spectrochemical Analysis & Instrumentation, Fujian Provincial Key Laboratory of Chemical Biology, and Department of Chemical Biology, College of Chemistry and Chemical Engineering, Xiamen University, Xiamen 361005, China;* ● orcid.org/0000-0003-3215-7013; Email: jhgao@ xmu.edu.cn

Authors

Yifan Fan − *The MOE Laboratory of Spectrochemical Analysis & Instrumentation, Fujian Provincial Key Laboratory of Chemical Biology, and Department of Chemical Biology, College of Chemistry and Chemical Engineering, Xiamen University, Xiamen 361005, China*

Limin Chen − *The MOE Laboratory of Spectrochemical Analysis & Instrumentation, Fujian Provincial Key Laboratory of Chemical Biology, and Department of Chemical Biology, College of Chemistry and Chemical Engineering, Xiamen University, Xiamen 361005, China*

Yuanxi Zheng − *The MOE Laboratory of Spectrochemical Analysis & Instrumentation, Fujian Provincial Key Laboratory of Chemical Biology, and Department of Chemical Biology, College of Chemistry and Chemical Engineering, Xiamen University, Xiamen 361005, China*

Ao Li − *The MOE Laboratory of Spectrochemical Analysis & Instrumentation, Fujian Provincial Key Laboratory of Chemical Biology, and Department of Chemical Biology,*

College of Chemistry and Chemical Engineering, Xiamen University, Xiamen 361005, China

Complete contact information is available at:
https://pubs.acs.org/10.1021/cbmi.3c00024

Author Contributions

Y.F. and L.C. contributed equally.

Notes

The authors declare no competing financial interest.

■ REFERENCES

(1) Rowe, S.; Pomper, M. Molecular imaging in oncology: Current impact and future directions. *CA Cancer J. Clin.* **2022**, *72* (4), 333−352.

(2) Savla, R.; Minko, T. Nanoparticle design considerations for molecular imaging of apoptosis: Diagnostic, prognostic, and therapeutic value. *Adv. Drug. Delivery Rev.* **2017**, *113*, 122−140.

(3) Yoshida, R.; Takagi, K.; Ishii, H.; Morishima, I.; Tanaka, A.; Morita, Y.; Kanzaki, Y.; Nagai, H.; Watanabe, N.; Furui, K.; Shibata, N.; Yoshioka, N.; Yamauchi, R.; Komeyama, S.; Sugiyama, H.; Tsuboi, H.; Murohara, T. Myocardial salvage after ST-segment-elevation myocardial infarction: Comparison between prasugrel and clopidogrel in the presence or absence of high-residual platelet reactivity. *J. Nucl. Cardiol.* **2021**, *28* (4), 1422−1434.

(4) Juweid, M.; Mueller, M.; Alhouri, A.; A-Risheq, M.; Mottaghy, F. Positron emission tomography/computed tomography in the management of Hodgkin and B-cell non-Hodgkin lymphoma. *Cancer* **2021**, *127* (20), 3727−3741.

(5) Yan, W.; Xu, H.; Jiang, L.; Zhang, L.; Guo, Y.; Li, Y.; Shen, L.; Min, C.; Yang, Z. Early longitudinal changes in left ventricular function and morphology in diabetic pigs: Evaluation by 3.0 T magnetic resonance imaging. *Cardiovasc. Diabetol.* **2023**, *22* (1), 6.

(6) Freund, P.; Seif, M.; Weiskopf, N.; Friston, K.; Fehlings, M.; Thompson, A.; Curt, A. MRI in traumatic spinal cord injury: from clinical assessment to neuroimaging biomarkers. *Lancet Neurol.* **2019**, *18* (12), 1123−1135.

(7) Tamaki, N.; Ajmera, V.; Loomba, R. Non-invasive methods for imaging hepatic steatosis and their clinical importance in NAFLD. *Nat. Rev. Endocrinol.* **2022**, *18* (1), 55−66.

(8) Zhou, Z.; Yang, L.; Gao, J.; Chen, X. Structure-relaxivity relationships of magnetic nanoparticles for magnetic resonance imaging. *Adv. Mater.* **2019**, *31* (8), 1804567.

(9) Lin, H.; Liu, K.; Gao, J. Surface engineering to boost the performance of nanoparticle-based T_1 contrast agents. *Eur. J. Inorg. Chem.* **2019**, *2019* (34), 3801−3809.

(10) Lin, H.; Tang, X.; Li, A.; Gao, J. Activatable ^{19}F MRI nanoprobes for visualization of biological targets in living subjects. *Adv. Mater.* **2021**, *33* (50), 2005657.

(11) Xie, D.; Yu, M.; Kadakia, R.; Que, E. ^{19}F magnetic resonance activity-based sensing using paramagnetic metals. *Acc. Chem. Res.* **2020**, *53* (1), 2−10.

(12) Dai, Y.; Xu, C.; Sun, X.; Chen, X. Nanoparticle design strategies for enhanced anticancer therapy by exploiting the tumour microenvironment. *Chem. Soc. Rev.* **2017**, *46* (12), 3830−3852.

(13) Zhao, Z.; Zhang, H.; Chi, X.; Li, H.; Yin, Z.; Huang, D.; Wang, X.; Gao, J. Silica nanovehicles endow arsenic trioxide with an ability to effectively treat cancer cells and solid tumors. *J. Mater. Chem. B* **2014**, *2* (37), 6313−6323.

(14) Wei, R.; Gong, X.; Lin, H.; Zhang, K.; Li, A.; Liu, K.; Shan, H.; Chen, X.; Gao, J. Versatile octapod-shaped hollow porous manganese-(II) oxide nanoplatform for real-time visualization of cargo delivery. *Nano Lett.* **2019**, *19* (8), 5394−5402.

(15) Li, A.; Luo, X.; Li, L.; Chen, D.; Liu, X.; Yang, Z.; Yang, L.; Gao, J.; Lin, H. Activatable multiplexed ^{19}F magnetic resonance imaging visualizes reactive oxygen and nitrogen species in drug-induced acute kidney injury. *Anal. Chem.* **2021**, *93* (49), 16552−16561.

(16) Ellis, C.; Pellico, J.; Davis, J. Magnetic nanoparticles supporting bio-responsive T_1/T_2 magnetic resonance imaging. *Materials (Basel)* **2019**, *12* (24), 4096.

(17) Low, L.; Wang, Q.; Chen, Y.; Lin, P.; Yang, S.; Gong, L.; Lee, J.; Siva, S.; Goh, B.; Li, F.; Ling, D. Microenvironment-tailored nanoassemblies for the diagnosis and therapy of neurodegenerative diseases. *Nanoscale* **2021**, *13* (23), 10197−10238.

(18) Jin, L.; Yang, C.; Wang, J.; Li, J.; Xu, N. Recent advances in nanotheranostic agents for tumor microenvironment-responsive magnetic resonance imaging. *Front. Pharmacol.* **2022**, *13*, 924131.

(19) Ovais, M.; Mukherjee, S.; Pramanik, A.; Das, D.; Mukherjee, A.; Raza, A.; Chen, C. Designing stimuli-responsive upconversion nanoparticles that exploit the tumor microenvironment. *Adv. Mater.* **2020**, *32* (22), 2000055.

(20) Kato, Y.; Ozawa, S.; Miyamoto, C.; Maehata, Y.; Suzuki, A.; Maeda, T.; Baba, Y. Acidic extracellular microenvironment and cancer. *Cancer cell int.* **2013**, *13* (1), 89.

(21) Dai, Y.; Xu, C.; Sun, X.; Chen, X. Nanoparticle design strategies for enhanced anticancer therapy by exploiting the tumour micro-environment. *Chem. Soc. Rev.* **2017**, *46* (12), 3830−3852.

(22) Guan, G.; Zhang, C.; Liu, H.; Wang, Y.; Dong, Z.; Lu, C.; Nan, B.; Yue, R.; Yin, X.; Zhang, X.; Song, G. Ternary alloy PtWMn as a Mn nanoreservoir for high-field MRI monitoring and highly selective ferroptosis therapy. *Angew. Chem., Int. Ed.* **2022**, *61* (31), No. e202117229.

(23) Zhao, Z.; Wang, X.; Zhang, Z.; Zhang, H.; Liu, H.; Zhu, X.; Li, H.; Chi, X.; Yin, Z.; Gao, J. Real-time monitoring of arsenic trioxide release and delivery by activatable T_1 imaging. *ACS Nano* **2015**, *9* (3), 2749−2759.

(24) Li, F.; Liang, Z.; Liu, J.; Sun, J.; Hu, X.; Zhao, M.; Liu, J.; Bai, R.; Kim, D.; Sun, X.; Hyeon, T.; Ling, D. Dynamically reversible iron oxide nanoparticle assemblies for targeted amplification of T_1-weighted magnetic resonance imaging of tumors. *Nano Lett.* **2019**, *19* (7), 4213−4220.

(25) Huang, X.; Huang, G.; Zhang, S.; Sagiyama, K.; Togao, O.; Ma, X.; Wang, Y.; Li, Y.; Soesbe, T.; Sumer, B.; Takahashi, M.; Sherry, A.; Gao, J. Multi-chromatic pH-activatable ^{19}F-MRI nanoprobes with binary ON/OFF pH transitions and chemical-shift barcodes. *Angew. Chem., Int. Ed.* **2013**, *52* (31), 8074−8.

(26) Guo, C.; Xu, S.; Arshad, A.; Wang, L. A pH-responsive nanoprobe for turn-on ^{19}F-magnetic resonance imaging. *Chem. Commun.* **2018**, *54* (70), 9853−9856.

(27) Zhang, P.; Zeng, J.; Li, Y.; Yang, C.; Meng, J.; Hou, Y.; Gao, M. Quantitative mapping of glutathione within intracranial tumors through interlocked MRI signals of a responsive nanoprobe. *Angew. Chem., Int. Ed.* **2021**, *60* (15), 8130−8138.

(28) Kim, M.; Son, H.; Kim, G.; Park, K.; Huh, Y.; Haam, S. Redoxable heteronanocrystals functioning magnetic relaxation switch for activatable T_1 and T_2 dual-mode magnetic resonance imaging. *Biomaterials* **2016**, *101*, 121−30.

(29) Nakamura, T.; Matsushita, H.; Sugihara, F.; Yoshioka, Y.; Mizukami, S.; Kikuchi, K. Activatable ^{19}F MRI nanoparticle probes for the detection of reducing environments. *Angew. Chem., Int. Ed.* **2015**, *54* (3), 1007−10.

(30) Tang, X.; Gong, X.; Li, A.; Lin, H.; Peng, C.; Zhang, X.; Chen, X.; Gao, J. Cascaded multiresponsive self-assembled ^{19}F MRI nanoprobes with redox-triggered activation and NIR-induced amplification. *Nano Lett.* **2020**, *20* (1), 363−371.

(31) Yue, R.; Zhang, C.; Xu, L.; Wang, Y.; Guan, G.; Lei, L.; Zhang, X.; Song, G. Dual key co-activated nanoplatform for switchable MRI

monitoring accurate ferroptosis-based synergistic therapy. *Chem.* **2022**, *8* (7), 1956−1981.

(32) Liu, J.; Yu, W.; Han, M.; Liu, W.; Zhang, Z.; Zhang, K.; Shi, J. A specific "switch-on" type magnetic resonance nanoprobe with distance-dominate property for high-resolution imaging of tumors. *Chem. Eng. J.* **2021**, *404*, 126496.

(33) Zhu, X.; Tang, X.; Lin, H.; Shi, S.; Xiong, H.; Zhou, Q.; Li, A.; Wang, Q.; Chen, X.; Gao, J. A fluorinated ionic liquid-based activatable ^{19}F MRI platform detects biological targets. *Chem.* **2020**, *6* (5), 1134−1148.

(34) Kadakia, R.; Xie, D.; Guo, H.; Bouley, B.; Yu, M.; Que, E. Responsive fluorinated nanoemulsions for ^{19}F magnetic resonance detection of cellular hypoxia. *Dalton Trans.* **2020**, *49* (45), 16419−16424.

(35) Kotas, M.; Medzhitov, R. Homeostasis, inflammation, and disease susceptibility. *Cell* **2015**, *160* (5), 816−827.

(36) Yang, B.; Chen, Y.; Shi, J. Reactive oxygen species (ROS)-based nanomedicine. *Chem. Rev.* **2019**, *119* (8), 4881−4985.

(37) Li, X.; Liu, Y.; Qi, X.; Xiao, S.; Xu, Z.; Yuan, Z.; Liu, Q.; Li, H.; Ma, S.; Liu, T.; Huang, Y.; Zhang, X.; Zhang, X.; Mao, Z.; Luo, G.; Deng, J. Sensitive activatable nanoprobes for real-time ratiometric magnetic resonance imaging of reactive oxygen species and ameliorating inflammation in vivo. *Adv. Mater.* **2022**, *34* (19), 2109004.

(38) Wang, H.; Yu, D.; Li, B.; Liu, Z.; Ren, J.; Qu, X. Ultrasensitive magnetic resonance imaging of systemic reactive oxygen species in vivo for early diagnosis of sepsis using activatable nanoprobes. *Chem. Sci.* **2019**, *10* (13), 3770−3778.

(39) Forman, H.; Zhang, H.; Rinna, A. Glutathione: Overview of its protective roles, measurement, and biosynthesis. *Mol.Aspects.Med.* **2009**, *30*, 1−12.

(40) Liu, K.; Kang, B.; Luo, X.; Yang, Z.; Sun, C.; Li, A.; Fan, Y.; Chen, X.; Gao, J.; Lin, H. Redox-activated contrast-enhanced T_1-weighted imaging visualizes glutathione-mediated biotransformation dynamics in the liver. *ACS Nano* **2021**, *15* (11), 17831−17841.

(41) Hu, Y.; Wang, Y.; Wen, X.; Pan, Y.; Cheng, X.; An, R.; Gao, G.; Chen, H.; Ye, D. Responsive trimodal probes for in vivo imaging of liver inflammation by coassembly and GSH-driven disassembly. *Research* **2020**, *2020*, 1−13.

(42) Myers, R. P.; Tainturier, M.-H.; Ratziu, V.; Piton, A.; Thibault, V.; Imbert-Bismut, F.; Messous, D.; Charlotte, F.; Di Martino, V.; Benhamou, Y.; Poynard, T. Prediction of liver histological lesions with biochemical markers in patients with chronic hepatitis B. *J. Hepatol.* **2003**, *39* (2), 222−230.

(43) Siraki, A. The many roles of myeloperoxidase: From inflammation and immunity to biomarkers, drug metabolism and drug discovery. *Redox Bio.* **2021**, *46*, 102109.

(44) Franchi, L.; Eigenbrod, T.; Muñoz-Planillo, R.; Nuñez, G. The inflammasome: a caspase-1-activation platform that regulates immune responses and disease pathogenesis. *Nat. Immunol.* **2009**, *10* (3), 241−7.

(45) Akazawa, K.; Sugihara, F.; Minoshima, M.; Mizukami, S.; Kikuchi, K. Sensing caspase-1 activity using activatable ^{19}F MRI nanoprobes with improved turn-on kinetics. *Chem. Commun.* **2018**, *54* (83), 11785−11788.

(46) Cui, L.; Hou, N.; Wu, H.; Zuo, X.; Lian, Y.; Zhang, C.; Wang, Z.; Zhang, X.; Zhu, J. Prevalence of Alzheimer's disease and Parkinson's disease in China: An updated systematical analysis. *Front. Aging Neurosci.* **2020**, *12*, 603854.

(47) Li, Y.; Li, Y.; Ji, W.; Lu, Z.; Liu, L.; Shi, Y.; Ma, G.; Zhang, X. Positively charged polyprodrug amphiphiles with enhanced drug loading and reactive oxygen species-responsive release ability for traceable synergistic therapy. *J. Am. Chem. Soc.* **2018**, *140* (11), 4164−4171.

(48) Tang, C.; Wang, Q.; Li, K.; Li, X.; Wang, C.; Xue, L.; Ju, C.; Zhang, C. A neutrophil-mimetic magnetic nanoprobe for molecular magnetic resonance imaging of stroke-induced neuroinflammation. *Biomater. Sci.* **2021**, *9* (15), 5247−5258.

(49) Wang, C.; Sun, W.; Zhang, J.; Zhang, J.; Guo, Q.; Zhou, X.; Fan, D.; Liu, H.; Qi, M.; Gao, X.; Xu, H.; Gao, Z.; Tian, M.; Zhang, H.; Wang, J.; Wei, Z.; Long, N. J.; Mao, Y.; Li, C. An electric-field-responsive paramagnetic contrast agent enhances the visualization of epileptic foci in mouse models of drug-resistant epilepsy. *Nat. Biomed. Eng.* **2021**, *5* (3), 278−289.

(50) Liu, J.; Chen, C.; Chen, H.; Huang, C.; Ren, Q.; Sun, M.; Tao, J.; Lin, B.; Zhao, P. Brain glucose activated MRI contrast agent for early diagnosis of Alzheimer's disease. *Anal. Chem.* **2022**, *94* (46), 16213−16221.